

Strontium isotopes trace the dissolution and precipitation of mineral organic carbon interactions in thawing permafrost

Arthur Monhonval^a, Catherine Hirst^a, Jens Strauss^b, Edward A.G. Schuur^c, Sophie Opfergelt^{a,*}

^a Earth and Life Institute, Université catholique de Louvain, Louvain-la-Neuve, Belgium

^b Permafrost Research Section, Alfred Wegener Institute Helmholtz Centre for Polar and Marine Research, Potsdam, Germany

^c Center for Ecosystem Society and Science, Northern Arizona University, Flagstaff, AZ, USA

ARTICLE INFO

Handling Editor: Alberto Agnelli

Keywords:

Permafrost
Thaw
Strontium isotopes
Mineral-associated organic carbon
Arctic
Iron oxides

ABSTRACT

Interactions between minerals and organic carbon (OC) in soils are key to stabilize OC and mitigate greenhouse gas emissions upon permafrost thaw. However, changes in soil water pathways upon permafrost thaw are likely to affect the stability of mineral OC interactions by inducing their dissolution and precipitation. This study aims to assess and quantify how mineral OC interactions are affected by dissolution and precipitation in thawed relative to unthawed layers. We hypothesize that a change in the radiogenic strontium (Sr) isotopic ratio ($^{87}\text{Sr}/^{86}\text{Sr}$) involved in mineral OC interactions upon changing water saturation conditions implies a destabilization of the mineral OC interaction. We quantified mineral OC interactions using selective extractions in soils facing gradual thaw (Eight Mile Lake, AK, USA) and in sediments with a thawing history of abrupt thaw (Duvanny Yar, Russia), and we measured the $^{87}\text{Sr}/^{86}\text{Sr}$ ratio of the selective extracts targeting the Sr associated to mineral OC interactions. Firstly, for water saturated layers with a higher proportion of mineral OC interactions, we found a difference in the $^{87}\text{Sr}/^{86}\text{Sr}$ ratio relative to the surrounding layers, and this supports the preservation of a Sr “stable” pool in these mineral OC interactions. We estimated that a portion of these mineral OC interactions have remained undissociated since their formation (between 4% and 64% by Sr isotope mass balance). Secondly, we found no difference in $^{87}\text{Sr}/^{86}\text{Sr}$ ratio between layers accumulating Fe oxides at redox interfaces regularly affected by water table changes (or upon thermokarst processes) relative to surrounding layers. This supports the dominance of a Sr “labile” pool inherited from processes of dissolution and precipitation of the mineral OC interactions. Thirdly, our estimations based on a Sr isotope mass balance support that, as a consequence of permafrost thaw, a larger proportion of Sr from primary mineral weathering (>80%) controls the Sr in mineral OC interactions in the saturated zone of deeply thawed soils relative to poorly thawed soils (~50%). In conclusion, we found that the radiogenic Sr isotope method, applied for the first time in this context, is promising to trace dissolution-precipitation processes of mineral OC interaction in thawing permafrost.

1. Introduction

Mineral organic carbon interactions provide a significant protective role for organic carbon (OC) in soils and sediments (von Lützow et al., 2006; Keil and Mayer, 2014; Kleber et al., 2015; 2021). Mineral-protected OC is known to be less available for microorganisms and is therefore less vulnerable to microbial degradation. In permafrost soils which store between 1,460 and 1,600 Pg C, twice the carbon stock currently found in the atmosphere, the OC enclosed in unfrozen and frozen layers below ground is highly sensitive to climate warming (Schuur et al., 2015; van Huissteden, 2020; Strauss et al., 2021).

Warming in northern latitudes is almost four times faster than the global warming rate and permafrost is currently thawing at an unprecedented rate (Fox-Kemper et al., 2021). The interactions between mineral surfaces or cations and OC act as a protective shield and reduce the portion of OC emitted as greenhouse gases in the atmosphere upon permafrost thaw (e.g., Mu et al., 2016; Herndon et al., 2017; Hemingway et al., 2019; Patzner et al., 2020). The temperature sensitivity of soil organic carbon is attenuated by mineral protection in permafrost soils (Gentsch et al., 2018).

The processes of dissolution and precipitation of such mineral OC interactions is a major concern to better predict future greenhouse gas

* Corresponding author.

E-mail address: sophie.opfergelt@uclouvain.be (S. Opfergelt).

<https://doi.org/10.1016/j.geoderma.2023.116456>

Received 4 August 2022; Received in revised form 21 March 2023; Accepted 25 March 2023

Available online 29 March 2023

0016-7061/© 2023 The Author(s). Published by Elsevier B.V. This is an open access article under the CC BY-NC-ND license (<http://creativecommons.org/licenses/by-nc-nd/4.0/>).

emissions upon gradual (i.e., deepening of the active layer) or abrupt (i.e., thermokarst processes) thaw in permafrost regions. Mineral OC interactions include aggregation, organo-mineral associations (involving Fe, Mn, Al oxides, clay minerals or carbonates) and organo-metallic complexes between polyvalent cations (e.g., Fe^{3+} , Al^{3+} , Ca^{2+}) and functional groups of organic acids. However, Fe oxides and organo-metallic complexes are known to be highly vulnerable with permafrost thaw due to changing soil conditions (Schwertmann, 1991; Colombo et al., 2014; Kleber et al., 2015; Winkler et al., 2018; Patzner et al., 2020). Permafrost thawing processes such as deepening of the active layer, thermokarst lake formation and drainage are responsible for changing soil moisture and water pathways in permafrost regions (Grosse et al., 2013; Vonk et al., 2019; Rodenhizer et al., 2020) and influence mineral OC interactions (Opfergelt, 2020; Monhonval et al., 2021b; 2022). Most permafrost-affected areas suffer from periodic or persistent anoxia due to soil water saturation (Street et al., 2016) which promotes the dissolution of Fe oxides and influences the formation of organo-metallic complexes (Schwertmann, 1991; Stumm and Sulzberger, 1992; Colombo et al., 2014; Kleber et al., 2015). The processes of dissolution and precipitation of mineral OC interactions may result from multiple freeze–thaw cycles inherited from changing soil conditions extending back thousands of years depending on sediment deposition processes and permafrost thawing history.

Determining what drives the preservation of mineral OC interactions or under what conditions mineral OC interactions are altered by dissolution and precipitation upon permafrost thaw is a challenge. In mineral OC interactions, calcium (Ca) can act (i) as a cation bridge adsorbed to Fe oxide surfaces or be occluded within Fe oxides structure and (ii) as a polyvalent metal cation participating in the formation of organo-metallic complexes (von Lützow et al., 2006; Kleber et al., 2015; Rowley et al., 2018). The role of Ca for organic complexation is generally promoted at neutral/alkaline pH (Rowley et al., 2018). The contribution of Ca to organo-metallic complexes should be quantified in mineral soil layers exposed by permafrost thaw relative to organic soil layers in surface, which are more acidic but enriched in Ca by plant cycling (Chapin et al., 1980). Strontium (Sr) is an alkaline earth metal of similar ionic size and charge as Ca and is established as an analogue for Ca (Faure and Powell, 1972; Capo et al., 1998). Because of their similar properties, Sr often substitutes to Ca, and can therefore be part of mineral OC interactions, i.e., occluded or adsorbed onto Fe oxides or complexed with organic acids (Andersson et al., 1994; Wortberg et al., 2017).

The radiogenic Sr isotope ratio ($^{87}\text{Sr}/^{86}\text{Sr}$) is commonly used as a source tracer in Earth surface processes (e.g., Miller et al., 1993; Capo et al., 1998; Banner, 2004). This results from a contrast between the rocks from the continental crust being more radiogenic (with a higher

$^{87}\text{Sr}/^{86}\text{Sr}$ ratio, i.e., enriched in ^{87}Sr which derives from ^{87}Rb decay) and the rocks from the mantle being less radiogenic (depleted in ^{87}Rb and therefore in ^{87}Sr). Strontium substitutes for Ca in Ca-bearing minerals such as plagioclase abundant in mantle rocks, whereas Rb substitutes for K in K-bearing minerals such as K-feldspar or muscovite (abundant in crustal rocks). Targeting Sr within the mineral OC interactions requires the selective extraction of Fe oxides and organo-metallic complexes in soils. This can be achieved using the dithionite-citrate-bicarbonate (DCB) extraction method commonly used to selectively extract Fe involved in Fe oxides (Mehra and Jackson, 1960) but which also extracts untargeted metals adsorbed to or occluded within Fe oxides or participating in organo-metallic complexes (Rennert, 2019).

In the context of permafrost thaw, we hypothesize that Sr within mineral OC interactions should display a “stable” pool that has not been submitted to dissolution processes since the formation of the mineral OC interaction. The $^{87}\text{Sr}/^{86}\text{Sr}$ in the “stable” Sr pool should reflect the Sr source from the time of the formation of the mineral OC interaction (Fig. 1). Conversely, we hypothesize the presence of a Sr “labile” pool within mineral OC interactions facing ongoing dissolution-precipitation with a $^{87}\text{Sr}/^{86}\text{Sr}$ reflecting the source of Sr from the time of the reprecipitation of the mineral OC interaction (Fig. 1). Since Sr is a highly soluble element (Gupta et al., 2018), the dissolution of mineral OC interactions should release Sr into the soil solution. Upon subsequent precipitation of the mineral OC interactions, Sr from the new soil solution with a potentially exogenous Sr source with a different Sr isotopic signature may co-precipitate with mineral OC interactions (Andersson et al., 1994) (Fig. 1). If this hypothesis is true, a similar Sr isotopic signature in mineral OC interactions before and after permafrost thaw (i.e., gradual thaw, thermokarst lake formation) would indicate that mineral OC interaction bonds with Sr are stable (no dissolution) or that the Sr from the new soil environment is characterized by a similar $^{87}\text{Sr}/^{86}\text{Sr}$ than the first Sr source (Fig. 1). However, a change in the $^{87}\text{Sr}/^{86}\text{Sr}$ within mineral OC interactions would suggest a dissolution step followed by the adsorption of Sr from a different source with a contrasting $^{87}\text{Sr}/^{86}\text{Sr}$ (Fig. 1). Considering that OC can be released together with Sr upon Fe oxide dissolution or organo-metallic complexes dissociation (von Lützow et al., 2006; Wortberg et al., 2017; Patzner et al., 2020), we use here Sr as a witness for the potential release of OC in changing water saturation conditions for mineral OC interactions upon thawing permafrost.

Upon gradual permafrost thaw, weatherable minerals bearing Sr from permafrost layers are exposed to water and can be dissolved and release Sr in the active layer (Kokelj et al., 2013; Reyes and Loughheed, 2015). Lateral transport in the saturated active layer may also provide Sr from an exogenous source with a distinct isotopic signature that differs from the Sr isotopic signature found in permafrost (Keller et al., 2007;

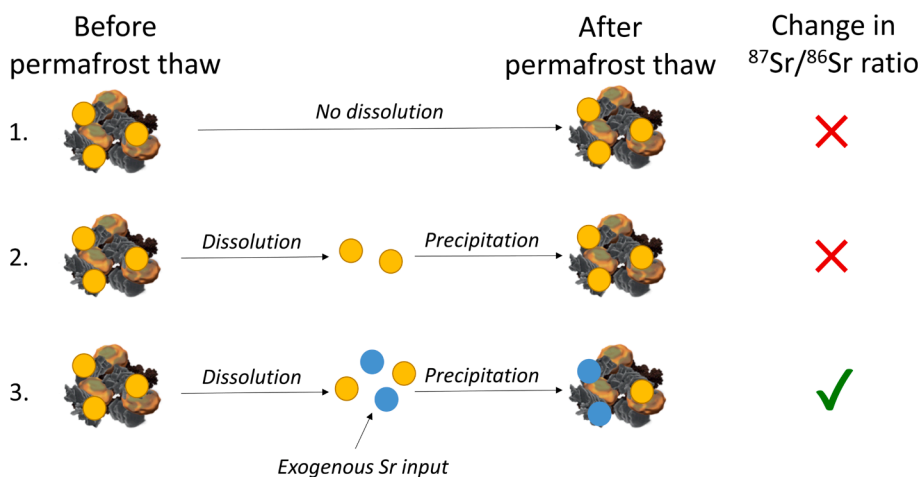


Fig. 1. Hypothesis on the stability of mineral organic carbon (OC) interactions upon permafrost thaw and the associated changes in $^{87}\text{Sr}/^{86}\text{Sr}$ ratio of the Sr occluded or adsorbed onto iron oxides and the Sr complexed with organic acids. Scenario 1: no dissolution of the mineral OC interactions and no change in $^{87}\text{Sr}/^{86}\text{Sr}$ ratio (“stable” Sr pool). Scenario 2: dissolution of the mineral OC interactions and subsequent precipitation with Sr of similar isotopic ratio (in yellow) than the first Sr source (“labile” Sr pool). Scenario 3: dissolution of the mineral OC interactions and subsequent precipitation with Sr from a different source (different isotopic ratio in blue) than the first Sr source (“labile” Sr pool).

2010; Hirst et al., 2022). Upon abrupt thaw, thermokarst lake formation and drainage during the Holocene can provide Sr from exogenous source with distinct isotopic signature compared to Yedoma deposits formed during the late Pleistocene (Biskaborn et al., 2013; Grosse et al., 2013). Therefore, both gradual and abrupt thaw can potentially modify the radiogenic Sr isotope ratio which allows to trace the stability of mineral OC interactions in thawing permafrost.

In this study, we use radiogenic Sr isotopes measured from DCB extracts in soils and sediments to trace dissolution-precipitation of mineral OC interactions upon thawing permafrost. To this aim, we investigate the changes in radiogenic Sr ratio of mineral OC interactions across a range of water saturation conditions between unthawed and thawed layers: (i) in a context of gradual thaw by comparing permafrost layers and active layers along a thaw gradient of permafrost soils with increasing active layer depth (including unsaturated and saturated active layers), and (ii) in a context of abrupt thaw by comparing sediment profiles from ice-rich Yedoma deposits that never thawed since

deposition during late Pleistocene and deposits that thawed during the Holocene (Alas and lake sediments).

2. Material and methods

2.1. Permafrost landscapes from Eight Mile Lake, Alaska, USA

The first site is a moist acidic tundra site located in Eight Mile Lake watershed, Healy, AK, USA (63.87°N, 149.25°W). Permafrost in this region is vulnerable to gradual thaw, deepening of the active layer, subsidence and water table level rise (Osterkamp et al., 2009; Plaza et al., 2019; Rodenhizer et al., 2020). The site is dominated by the tussock forming sedge (*Eriophorum vaginatum*), various small shrubs and *Sphagnum* spp. mosses (Schuur et al., 2007; Mauclet et al 2022; Villani et al 2022). Soils are Histic Turbic Cryosols (IUSS Working Group WRB, 2015). The modern active layer at this site (0–66 cm) spans a range from 0 – 4.6 ka (i.e., thousand years) and the underlying permafrost layer

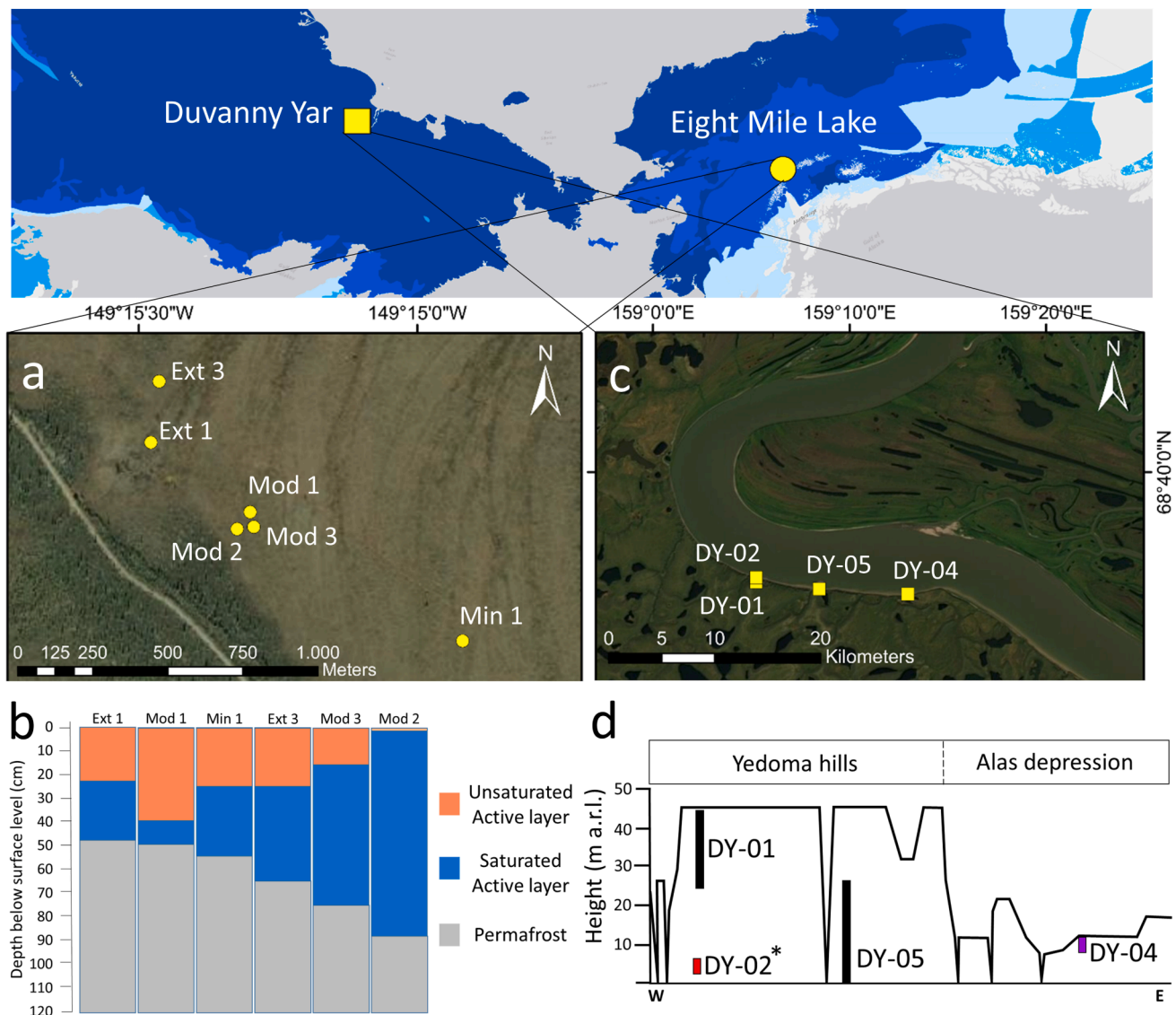


Fig. 2. (a) Location of Eight Mile Lake, Healy, AK, USA and the six soil profiles collected (yellow points); (b) Schematic of the six profiles investigated at Eight Mile Lake with the thickness of the unsaturated and saturated active layer (orange and blue, respectively) and the permafrost (gray) (soil profiles by increasing active layer depth Ext1 < Mod1 < Min1 < Ext3 < Mod3 < Mod2 sampled along a thaw gradient originally defined as minimal (Min), moderate (Mod), and extensive (Ext) permafrost degradation; Table S1); (c) Location of Duvanny Yar, Kolyma Lowland, Siberia, Russia and the four sediment profiles collected (yellow squares); (d) Schematic of the Duvanny Yar section with position (m. a.r.l. = height above river level) of the studied profiles (modified from Strauss (2010)): Yedoma deposits are represented in black (DY-01 and DY-05), Alas deposits in purple (DY-04) and Lake sediments in red (DY-02). *DY-02 is a separate profile underlying the Yedoma deposits sequence. Maps were built with ArcGIS software; source: Esri, DigitalGlobe, GeoEye, USDA, USGA, IGN and the GIS User community.

(66–123 cm) spans a range from 4.6 to 15 ka (Hutchings et al., 2019). This site is ideal to test potential dissolution-precipitation processes of mineral OC interactions along a permafrost thaw gradient. The original thaw gradient was defined >30 years ago with minimal (Min), moderate (Mod), and extensive (Ext) permafrost degradation (Osterkamp et al., 2009). Since then the gradient has evolved resulting in variable active layer thickness at the site (Schuur et al., 2021). We have selected six soil profiles of increasing active layer depth (Ext1 < Mod1 < Min1 < Ext3 < Mod3 < Mod2; Fig. 2a-b; Table S1). The six profiles were sampled by layer ($n = 72$ individual horizon-level soil samples) at time of deepest active layer depth (late August 2019), using a knife in the upper part of the profile and a stainless-steel pipe manually hammered down below the water table (Palmtag et al., 2016). Permafrost was reached for every core and up to a maximum depth of 120 cm. The active layer thickness varied with microtopography and ranges from 48 cm to 88 cm and the water table depth ranges between 0 and 40 cm (Table S2). All samples were air-dried. Samples from the litter were shredded without sieving while other samples were sieved at 2 mm to remove the roots (absence of coarse fragments) and ground prior to laboratory analyses. These soil profiles have been characterized for their total organic carbon (TOC) content (Mauclet et al. (2023); Fig. S1).

2.2. Permafrost landscapes from Duvanny Yar, Yakutia, Russia

The second site is an ice-rich permafrost site from Duvanny Yar in the Kolyma Lowland, Siberia, Russia (68.63 °N, 159.10 °E; located in the Yedoma domain as defined by Strauss et al. (2017)). This site is affected with thermokarst lake formation and drainage. The Duvanny Yar site is considered to be a key site for late Pleistocene history and has a long history of study since 1950's (Popov, 1953; Tomirdiario and Chernen'kiy, 1987; Rozenbaum and Shpolyanskaya, 1998; Zanina et al., 2011; Strauss et al., 2012; Murton et al., 2015). Duvanny Yar silty sediments from the Yedoma profiles are characterized as polygenetic and loess-related deposits (Strauss et al., 2012; Murton et al., 2015; Shmelev et al., 2021). The mineralogy of this deposit is characterized by the presence of pyroxene, hornblende, pyrope, magnetite, goethite, quartz, feldspar, calcite, illite, and chlorite (Shmelev et al., 2021). Samples were collected from an approximately 12-km-long outcrop, which consists of Yedoma hills as high as 50 m above river level (a.r.l.) dissected by deep thermo-erosional valleys and thermokarst depressions exposed along the Kolyma river (Fig. 2c-d). This late Pleistocene syngenetic permafrost is vulnerable to abrupt thaw (i.e., thermokarst lake formation and drainage) and is also well suited to test the dissolution-precipitation dynamic of mineral OC interactions. Duvanny Yar Yedoma deposits span a range from >45 ka to 9 ka for uppermost Holocene sediments (Strauss, 2010). A total of 46 samples from two Yedoma profiles (DY-01 and DY-05) and two previously thawed profiles (one lake sediment profile (DY-02) and one Alas profile (DY-04)) were collected using hand-held drill or hammer after cleaning the first centimeters of the outcrop (Table S1). The samples were air-dried, and no sieving was necessary given that the particle size distribution of these Yedoma domain deposits is below 2 mm (Strauss, 2010). These samples for which the TOC content is available (Table S2; Fig. S2) represent a subset of the full profiles from this site studied in Monhonval et al. (2021b) (Fig. S3).

2.3. Selective Fe, Sr and Ca extraction

The concentrations of Fe and Sr selectively extracted by dithionite-citrate-bicarbonate (DCB; Mehra and Jackson, 1960) were determined on all samples from Eight Mile Lake study site ($n = 72$) and Duvanny Yar site ($n = 46$) (Table S2). Briefly, 0.75 g of finely ground soil or sediment sample was mixed with 30 ml of citrate solution (sodium citrate $\text{Na}_3\text{C}_6\text{H}_5\text{O}_7 \cdot 2\text{H}_2\text{O}$) 0.3 M buffered by sodium bicarbonate NaHCO_3 in centrifugal tubes. The dithionite (three to five times 0.75 g) was added to the tubes placed in a hot bath at 85 °C while stirring. The DCB-extract was filtered (Whatman 41 filter, 20 μm retention size) and the Fe and Sr

concentrations were measured by inductively coupled plasma optical emission spectrometry (ICP-OES, iCAP 6500 Thermo Fisher Scientific). The precision (coefficient of variation) of the ICP-OES measurement on permafrost samples is 0.5% and 1% for Fe and Sr, respectively (Monhonval et al., 2021a) and limit of detection was never reached (0.004 mg L^{-1} and 0.0001 mg L^{-1} for Fe and Sr, respectively). The concentration of DCB-extracted Fe and Sr is expressed in reference to the soil or sediment dry weight (105 °C) and will be referred as Fe_d and Sr_d (in mg kg^{-1}) in the following.

The proportion of DCB-extracted Sr over the total Sr concentration ($\text{Sr}_d/\text{Sr}_{\text{total}}$) was determined by measuring the total Sr concentrations in the bulk samples (Eight Mile Lake site, $n = 72$; Duvanny Yar site, $n = 46$; Table S2) by portable X-ray fluorescence (pXRF) device and corrected using a regression with measurements by ICP-OES after alkaline fusion following the method described in Monhonval et al. (2021) (Fig. 3; $R^2 = 0.99$).

The concentration of Ca selectively extracted by Na-pyrophosphate was determined on the samples from Eight Mile Lake study site ($n = 72$; Table S2). This site presents contrast between samples with <20% TOC and >40% TOC to investigate the role of Ca on organic complexes, whereas the Duvanny Yar site only presents samples with TOC < 20%. Practically, 0.4 g of milled sample was mixed with 40 ml of pyrophosphate solution (tetrasodium pyrophosphate decahydrate $\text{Na}_4\text{P}_2\text{O}_7 \cdot 10\text{H}_2\text{O}$ 0.1 M). The tube was agitated for 16 h. Sodium sulfate (1.4 g) was added and the solution was centrifuged (30 min at 4,000 rpm) and filtered (Whatman 41 filter). This extraction is presumed to target Ca involved in organo-metallic complexes and also dispersible colloids (Bascomb, 1968; Parfitt and Childs, 1988). The Ca concentrations in these extracts were analyzed by ICP-OES (iCAP 6500 Thermo Fisher Scientific), expressed in reference to the soil dry weight at 105 °C (mg kg^{-1}), and will be referred as Ca_p in the following.

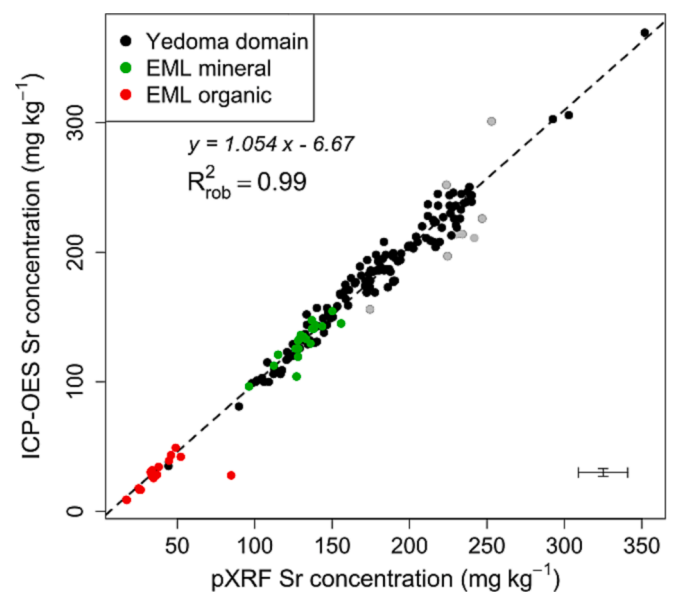


Fig. 3. Total Sr concentrations (mg kg^{-1}) measured by the inductively coupled plasma optical-emission spectrometry (ICP-OES) method as a function of those measured by the portable X-ray fluorescence (pXRF) method on mineral and organic samples from Eight Mile Lake acidic tundra (green points; $n = 21$ and red points $n = 18$, respectively). Samples from the Yedoma domain deposits (black points; $n = 144$, Monhonval et al. (2021)) are included. The robust linear regression for mineral and organic samples is presented (dashed black line; $\alpha = 0.95$). Grey points are excluded from the robust linear regression. Mineral and organic samples are divided with 20 wt% organic carbon cutoff (Hicks Pries et al., 2012). Equation from linear regressions is provided with the robust determination coefficient. Errors bars ($\pm 2\sigma$) are taken from Monhonval et al. (2021).

2.4. Purification of Sr and radiogenic Sr isotope measurements

The radiogenic Sr isotopic ratio of the DCB extracts (section 2.3) has been measured for all samples from Eight Mile Lake study site ($n = 72$) and Duvalny Yar site ($n = 46$). A volume of DCB extract corresponding to 500 ng of Sr was evaporated in Teflon vials on a hot plate (50 °C). The sample was then mixed with H₂O₂ and concentrated HNO₃ to remove organics: the sample reacted in sealed Teflon vials on a hot plate (180 °C) and was then evaporated to dryness. This step was repeated 2 to 3 times. To purify Sr from the sample, the aliquot was dissolved in 3 M HNO₃ and loaded on a Biorad microspin column containing 500 µl of Sr specific resin (50–100 µm Triskem), and eluted in several stages with HNO₃ (Aciego et al., 2009). The sample containing the purified Sr was evaporated to dryness and dissolved in HNO₃ 2% for Sr isotope measurements. The total procedural Sr blank was <0.1% of the total Sr analyzed.

Strontium isotope measurements were carried out by MC-ICP-MS (Neptune Plus TM High Resolution Multicollector ICP-MS, Thermo Fisher Scientific, Earth and Life Institute, UCLouvain, Belgium) in wet plasma mode using a PerFluoroAlkoxy (PFA) nebulizer of 100 µl min⁻¹ uptake rate. Typical sensitivity for 100 ppb Sr was about 7 V. Each sample was measured with three repetitions and the results are expressed as ⁸⁷Sr/⁸⁶Sr ratio (average ± 2SD on the three repetitions). The long-term precision and accuracy was assessed using an in-house standard Sr ICP (0.708598 ± 0.000115; 2SD, $n = 75$) and the reference material NIST SRM987 (0.710303 ± 0.000033; 2SD, $n = 20$), consistent with certified value for this reference material (0.71034 ± 0.00026; Standard Reference Material® 987, Strontium Carbonate, Isotopic Standard). The NIST SRM987 reference material was also used to validate that no interference was associated to the DCB matrix. The obtained value for the ⁸⁷Sr/⁸⁶Sr ratio after mixing the NIST SRM987 with DCB and column purification was 0.710313 ± 0.000073 (2SD, $n = 27$), also consistent with the certified value (0.71034 ± 0.00026).

The radiogenic Sr isotope ratio is a tool that can be used in mixing models to estimate the proportion of Sr in a specific layer that combines a more radiogenic source from upper soil layer with a less radiogenic

source from deeper soil layers. This mixing tool can be used to estimate quantitatively the proportion of Sr preserved in a specific layer accumulating mineral OC interactions in the saturated soil layers. For instance, in EML, we can use the average ⁸⁷Sr/⁸⁶Sr ratio from unsaturated soil layer (Sr ratio_{Unsaturated} = 0.7095897; section 3.1) and from permafrost layer (Sr ratio_{Permafrost} = 0.7087378; section 3.1) as end-member values to estimate their contribution to a specific layer from the saturated layer using the following equation (Eq.1):

$$Sr\ ratio_{Saturated} = X * Sr\ ratio_{Permafrost} + (1 - X) * Sr\ ratio_{Unsaturated} \quad (1)$$

where X refers to the contribution of permafrost Sr source in the specific saturated layer of interest.

2.5. Statistical data treatment

Correlation analysis using Pearson method between parameters were constructed using *corrplot* package. To assess statistical differences between two datasets, we performed the Wilcoxon test. All statistics were performed using R core software (R Core Team, 2018).

3. Results

3.1. Eight Mile Lake site: Concentrations in Fe, Sr, Ca and ⁸⁷Sr/⁸⁶Sr ratio in selective extracts from the soil profiles

The concentration in DCB-extracted Fe of Eight Mile Lake soils ranges between 1.02 and 75.0 g kg⁻¹ with the highest recorded values at the water table (Fig. 4). About 51% of total Sr is DCB-extractable (Sr_d/Sr_{total}) in organic samples and can be associated to mineral OC interactions (Fig. S4; Fig. S5a). This percentage substantially decreases to 6.8% in mineral samples (Fig. S4; considering Fig. S1 to differentiate organic (TOC > 20%) from mineral samples (TOC < 20%; Hicks Pries et al. (2012)). Note that the concentration of Sr_d is lower in deeper soil and that a significant amount of Sr from deeper soil layers would be needed to slightly change the Sr isotopic ratio in DCB-extracted solution from surface soils. The concentrations in Ca selectively extracted by

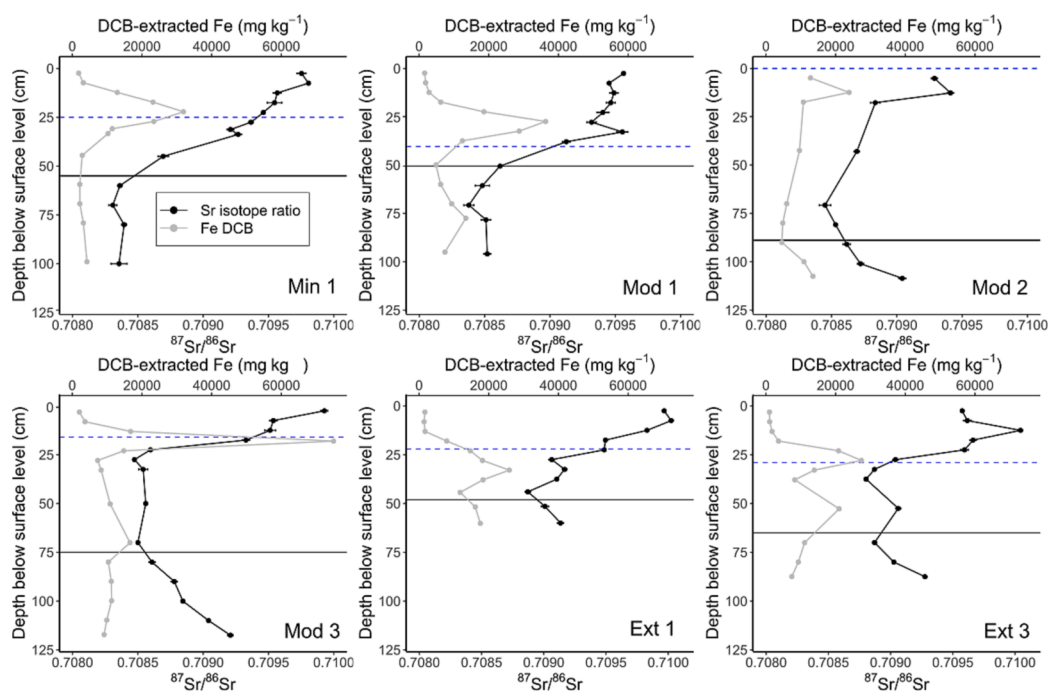


Fig. 4. Radiogenic Sr isotopic ratio from DCB extraction (⁸⁷Sr/⁸⁶Sr; black points, bottom x-axis) and concentration in dithionite-citrate-bicarbonate (DCB) extracted Fe (in mg kg⁻¹; gray points, top x-axis) for Eight Mile Lake soil profiles Min 1 (a), Mod 1 (b), Mod 2 (c), Mod 3 (d), Ext 1 (e) and Ext 3 (f). Errors bars (±2SD) are represented for radiogenic Sr isotopic ratio. The water table (dashed blue line) and permafrost table (black line) are represented for each plot.

pyrophosphate (Ca_p) ranges from 369 and 3233 mg kg^{-1} (Table S2). Our results indicate a positive correlation ($r = 0.98$) for all samples (except unsaturated active layer samples) between the DCB-extracted Sr and the pyrophosphate-extracted Ca (Fig. 5a).

In the moist acidic tundra site of Eight Mile Lake, the $^{87}\text{Sr}/^{86}\text{Sr}$ ratio of the DCB extracts ranges between 0.708309 and 0.710044 (Fig. 4). Samples from the organic-rich layer ($n = 37$) are significantly more radiogenic than samples from mineral layers ($n = 35$; p -value < 0.001 ; Fig. S6a). The maximum $^{87}\text{Sr}/^{86}\text{Sr}$ ratio in DCB extracts is often found within the first 15 cm depth of tundra soils. In addition, a significant decrease in the Sr ratio is observed between active layer and permafrost (p -value < 0.001 , $n = 51$ and 21 for permafrost and active layer, respectively). Within the permafrost, the radiogenic Sr ratio of the DCB extracts is constant with depth in profiles Min 1 and Mod 1 but increases with depth in all other profiles (Fig. 4c-f). Despite the increase in permafrost layers, the radiogenic Sr ratio of the DCB extracts is the highest in top surface horizons which allows us to decipher two isotopic signatures, one from the unsaturated layer (0.709590) and one from deeper frozen layers (0.708739). The $^{87}\text{Sr}/^{86}\text{Sr}$ ratio in the DCB extracts found in top of the waterlogged profile with deepest thaw (0.709288; 0–10 cm) is lower compared to top surface layer from adjacent profile (Mod1 and Mod3; Fig. 4). Overall, a positive correlation is found between $^{87}\text{Sr}/^{86}\text{Sr}$ ratio of the DCB extracts and the TOC ($r = 0.81$; Fig. S6a). In the unsaturated active layer, the $^{87}\text{Sr}/^{86}\text{Sr}$ ratio of the DCB extracts and the amount of Fe involved in Fe oxides or participating in organo-metallic complexes (Fe_d concentrations; Fig. 4 and Fig. S6c) are negatively correlated ($r = -0.58$; Fig. S6c), whereas these two variables are positively correlated in the saturated active layer and the permafrost ($r = 0.52$; Fig. S6c). Our results also indicate a positive correlation between the $^{87}\text{Sr}/^{86}\text{Sr}$ ratio of the DCB extracts and the pyrophosphate-extracted Ca ($r = 0.77$; Fig. 5b), with the highest Sr isotopic ratio found in unsaturated soil layers.

3.2. Duvanny Yar site: Concentrations in Fe, Sr and $^{87}\text{Sr}/^{86}\text{Sr}$ ratio in selective extracts from the sediment profiles

The concentration in DCB-extracted Fe in Duvanny Yar sediments ranges between 7.76 and 52.8 g kg^{-1} (Fig. 6). The highest values are found as a narrow accumulation (< 50 cm thick; Fig. 6) in the thawed and refrozen deposits (DY-04 and DY-02 profiles). About 10% of total Sr is DCB-extractable with a range of 5 to 26% and the maximum found in an organic-rich layer of the Yedoma deposits (DY-01, 29 m a.r.l.; Fig. S5b; Fig. S7).

Both Yedoma deposit profiles span an identical range of DCB extracted $^{87}\text{Sr}/^{86}\text{Sr}$ ratio (0.709175 ± 0.000426 and 0.708980 ± 0.000221 ; mean \pm 2SD for DY-01 and DY-05, respectively; Fig. 6). Similarly, the $^{87}\text{Sr}/^{86}\text{Sr}$ ratio in DCB extracts of Alas deposits and Lake sediment profile falls within similar range as the Yedoma profiles. The Alas profile (DY-04) shows a $^{87}\text{Sr}/^{86}\text{Sr}$ ratio of 0.708988 ± 0.000206 and the lake sediment profile (DY-02) a $^{87}\text{Sr}/^{86}\text{Sr}$ ratio of 0.709099 ± 0.000485 . The highest Sr isotopic ratios in DCB extracts are found in peat layers from the Yedoma (DY-01) and the lake sediments profile (DY-02; Fig. 6; Fig. S6a).

4. Discussion

4.1. Controls on the variability of the radiogenic Sr ratio in mineral OC interactions from Eight Mile Lake soil profiles

4.1.1. General soil profile

We observe a general decrease in the $^{87}\text{Sr}/^{86}\text{Sr}$ ratio of the DCB-extracted Sr from surface to depth in the soil profiles from Eight Mile Lake (Fig. 4). This is consistent with previous studies from other permafrost regions which highlighted similar decrease in radiogenic Sr ratio in deeper soil layers relative to top surface layer (Keller et al., 2010; Bagard et al., 2013). The mineralogy of Eight Mile Lake tundra soil is derived from loess that accumulated during the late Pleistocene and Holocene period which is characterized by minerals such as K-feldspar, micas, illitic clay minerals (i.e., K-rich more radiogenic minerals), but

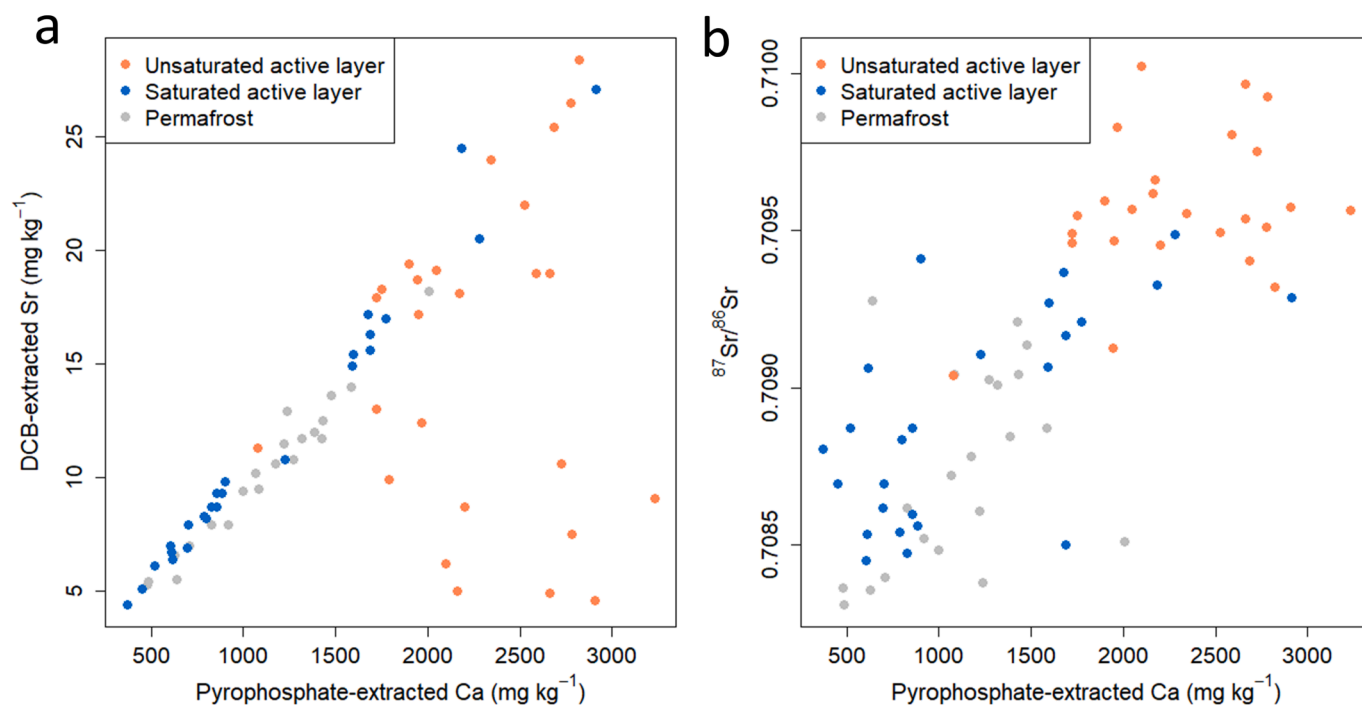


Fig. 5. For unsaturated active layer (orange), saturated active layer (blue) and permafrost (gray) samples from Eight Mile Lake soils: (a) Concentration of dithionite-citrate-bicarbonate (DCB) extracted Sr as a function of pyrophosphate-extracted Ca (mg kg^{-1}); (b) Radiogenic Sr isotopic ratio ($^{87}\text{Sr}/^{86}\text{Sr}$) of the DCB extracts as a function of pyrophosphate-extracted Ca (mg kg^{-1}).

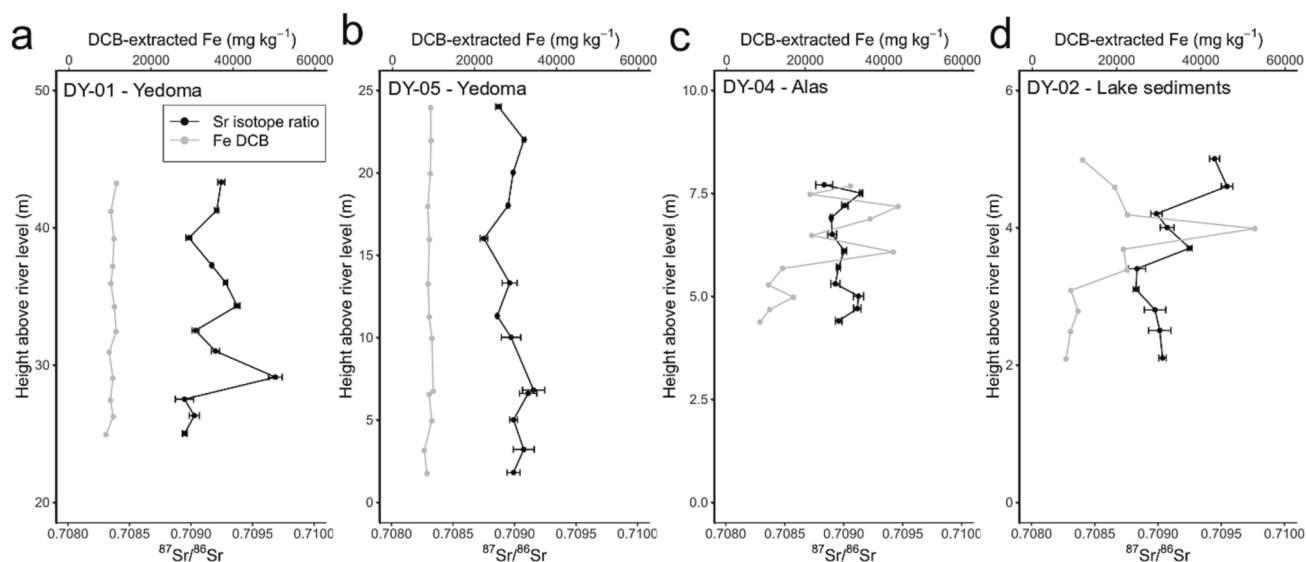


Fig. 6. Radiogenic Sr isotopic ratio from dithionite-citrate-bicarbonate (DCB) extraction ($^{87}\text{Sr}/^{86}\text{Sr}$; black points, bottom x-axis) and concentration in dithionite-citrate-bicarbonate (DCB) extracted Fe (in mg kg^{-1} ; gray points, top x-axis) for Duvanny Yar sediment profiles DY-01 (a), DY-05 (b), DY-04 (c) and DY-02 (d). The two Yedoma profiles are displayed on the left (a and b). The Alas profile (c) and lake sediment profile (d) on the right. Errors bars ($\pm 2\text{SD}$) are represented for radiogenic Sr isotopic ratio.

also plagioclase and other Ca-bearing minerals (i.e., Ca-rich less radiogenic minerals) (Mauclet et al., 2023). The difference in radiogenic Sr isotopic composition with depth likely reflects a higher proportion of K-rich minerals (i.e., characterized with a high $^{87}\text{Sr}/^{86}\text{Sr}$ ratio) in the upper soil profile relative to a higher proportion of Ca-rich minerals (characterized with a low $^{87}\text{Sr}/^{86}\text{Sr}$ ratio) in the lower soil profile. This can be explained by dissolution of the more weatherable Ca-plagioclase and the relative increase in resistant K-rich minerals in the uppermost soil layers, thereby resulting in higher $^{87}\text{Sr}/^{86}\text{Sr}$ ratio in organo-rich layers in the upper part of the profile (Drouet et al., 2007).

Atmospheric deposition is another process which could enrich surface soil horizons with exogenous inorganic rock-derived Sr and contribute to Sr release for mineral OC interactions (Graustein and Armstrong, 1983; Derry and Chadwick, 2007). While Sr derived from marine aerosol was reported as an important source of Sr in some highly weathered and/or coastal systems (Graustein and Armstrong, 1983; Chadwick et al., 2009; Pearce et al., 2015), the influence of marine deposition is negligible in the continental environment of Interior Alaska (Hirst et al., 2022) and is therefore neglected in this study.

4.1.2. Specific soil layers

In unsaturated active layers, according to the absence of correlation between Fe_d concentration and $^{87}\text{Sr}/^{86}\text{Sr}$ ratios (Fig. 4 and Fig. S6c), the increase in mineral OC interactions involving Fe do not influence the Sr isotopic ratio of the DCB extracts. This supports that mineral OC interactions involved in these soils are not only controlled by interactions with Fe. Mineral OC interactions can involve organo-metallic complexes with elements such as Ca, and hence Sr, as supported by higher $\text{Sr}_d/\text{Sr}_{\text{Total}}$ in unsaturated soil layers (Fig. S4). The positive correlation between the DCB-extracted Sr and the pyrophosphate-extracted Ca ($r = 0.98$), better than between the DCB-extracted Sr and the DCB-extracted Fe ($r = 0.58$), for all samples (except unsaturated active layer samples; Table S2) supports the existence of organo-metallic complexes with Sr^{2+} substituting for Ca^{2+} in Eight Mile Lake soils. Even if the contribution of Ca to organic complexation is generally promoted at neutral/alkaline pH (Rowley et al., 2018), the data support a contribution from Ca to organic complexation in mineral horizons (lower part of the active layer and permafrost: $\text{pH } 5.2 \pm 0.6$; Mauclet et al., 2023) and in organic horizons (upper part of the active layer: $\text{pH } 4.0 \pm 0.2$; Mauclet et al., 2023). The Ca contribution to OC complexation in organic horizons is likely related

to plant cycling (Chapin et al., 1980) with evidence for Ca accumulation in the organic horizons at the study site (e.g., Mauclet et al., 2022; Villani et al., 2022). The higher Sr isotopic ratio with higher organo-metallic complexes with Ca (Fig. 5b) is likely explained by the location of the sample in the top surface layer of Eight Mile Lake tundra soils. Indeed, the high Sr isotopic ratio in unsaturated layers can be explained by the contribution from secondary minerals in the organic layer as a source of Sr, as observed for the exchangeable Sr (Mauclet et al., 2023).

An accumulation of mineral OC interactions (higher concentrations in Fe_d) is usually found close to the redox interface (Fig. 4). We argue that the Fe_d accumulation location indicates the mean position of the water table fluctuation level during summer season for each specific soil profile (i.e., the water table level displayed on the plots refers to the water table at the moment of sampling; Fig. 4). The Sr within such mineral OC interactions can be Sr adsorbed or occluded to Fe oxides or Sr involved in organo-metallic complexes. Here, the positive correlation in saturated soil layers between the concentration in DCB-extracted Sr and the organo-metallic complexes with Ca^{2+} (pyrophosphate-extracted Ca; Ca_p) ($r = 0.99$; Fig. 5a) indicate a high proportion of organo-metallic complexes with Sr. The divalent cation Sr^{2+} , like Ca^{2+} is potentially able to stabilize the negative charge of polyfunctional groups in organic acids. However, the accumulation of mineral OC interactions near the redox interface do not modify the overall $^{87}\text{Sr}/^{86}\text{Sr}$ ratio of that layer compared to the surrounding soil layers (i.e., located directly above or below; Fig. 4). This can be explained by a large pool of labile Sr submitted to repeated dissolution-precipitation cycles or by the increased abundance of organo-metallic complexes with dynamic association-dissociation processes. The interface between minerals and organic carbon evolves continuously with changes in the chemistry of aqueous phases, organic matter and mineralogy, and influences both magnitude and rate of OC adsorption (Kleber et al., 2021). This dynamic exchange between the mineral and organic compounds may be greater within organo-metallic complexes compared to spatially occluded Sr within Fe oxides (von Lütow et al., 2006). The mineral OC interactions found at the redox interface are substantial but our results indicate a poor stability in time of these interactions and rather highly dynamic cycles of dissolution-precipitation leading to a radiogenic Sr isotope ratio reflecting the last Sr source available in that specific soil layer.

The Fe accumulation at the water table is commonly explained with the hypothesis that Fe^{2+} is released from weathered minerals previously

locked in permafrost which migrates upward towards oxic zones before oxidation and precipitation as poorly crystalline oxides or as organo-metallic complexes (Lipson et al., 2012; Herndon et al., 2017; Patzner et al., 2022). Another explanation could be that soluble organo-metallic complexes present in permafrost or formed above the permafrost table migrate upwards with water table fluctuations and settle at the redox interface. In the first scenario, Fe^{2+} mobility is independent of Sr because they are not interacting. The Sr adsorbed at the time of Fe oxidation is therefore the one found locally at the redox interface with a high $^{87}\text{Sr}/^{86}\text{Sr}$ ratio. This first scenario would not modify the Sr isotopic signature of DCB extracts at the water table because Sr would originate from top surface layer close to the redox interface. In the second scenario, Sr is translocated upward together with soluble organo-metallic complexes. Under these conditions, the $^{87}\text{Sr}/^{86}\text{Sr}$ ratio of DCB extracts at the Fe accumulation layer would decrease reflecting less radiogenic Sr from deeper source mixing with more radiogenic Sr from upper soil layer. Here, the results suggest that the first scenario is the more likely and that there is no mixing of Sr from deeper layers upon gradual thaw. In terms of organic carbon stabilization, this supports that mineral OC interactions must be disrupted on ascent and cannot migrate in a stable form towards the redox interface. Organic carbon is therefore more vulnerable upon Fe oxide dissolution in long-term saturated soil conditions with low potential to form mineral OC interactions.

In saturated active layers, the radiogenic Sr isotopic signature of DCB extracts and Fe_d concentration are positively correlated ($r = 0.65$; Fig. S6b). As an example, the slight increase in Fe_d concentration below the water table level in the profile Mod 2 (10–15 cm; Fig. 4c) is concomitant with an increase in radiogenic Sr isotopic signature. Similarly, below the water table level of profiles Ext 1 and Ext 3, the higher Fe_d concentrations result in higher radiogenic Sr isotopic signature (Fig. 4e, f). These locally different $^{87}\text{Sr}/^{86}\text{Sr}$ ratios in DCB extracts for Fe_d enriched likely reflect the Sr isotopic signature preserved in a Sr “stable” pool induced by the higher proportion of mineral OC interactions (section 4.3.1). Future work designed to probe redox-sensitive dynamics specifically, such as the influence of newly precipitated Fe associated OC on the variability of the $^{87}\text{Sr}/^{86}\text{Sr}$ ratios in DCB extracts, would be valuable to the approach.

4.2. Controls on the variability of the radiogenic Sr ratio in mineral OC interactions from Duvanny Yar sediment profiles

4.2.1. General sediment profile

We found that DCB-extracted Fe concentration was homogeneous with depth in both Yedoma profiles but more variable with depth in Alas deposits (DY-04) and Lake sediments (DY-02) (Fig. 6). These data support that, compared to Yedoma deposit profiles, Fe oxides and organo-metallic complexes are redistributed upon thermokarst process leading to layers of accumulation of mineral OC interactions in Alas and Lake sediment profiles (Fig. 6). This is supported by the redistribution of total Fe concentration upon thermokarst processes highlighted in Monhonval et al. (2021b), between the homogeneous Fe concentration in Yedoma profiles and the highly variable Fe concentration in Alas and Lake sediment profile (Fig. S3). However, the higher Fe_d concentration in previously thawed deposits compared to Yedoma deposits is not correlated with higher Sr isotopic ratio of the DCB extracts (Fig. S6d).

The identical radiogenic Sr signature of the DCB extracts in both Yedoma deposits profile was expected and is explained by the similar loess origin upon Yedoma formation during the late Pleistocene. Both Yedoma profiles were submitted to similar cold and dry climate conditions and therefore, Yedoma deposits were very likely to display identical $^{87}\text{Sr}/^{86}\text{Sr}$ reflecting their similar sources. Grain size analysis from Strauss et al. (2012) indicates stable sediment sources and persistent transport conditions with very likely loess origin (grain size distribution with a large peak at 20 to 60 μm ; Smalley and Smalley, 1983). In addition, Yedoma deposits from the Kolyma Lowland and elsewhere are characterized by weak intensity of chemical weathering because of their

specific mineralogy, continental origin, cold and arid climate conditions (Aleksiev et al., 2003). The lack of chemical weathering could be partially responsible for the rather homogeneous $^{87}\text{Sr}/^{86}\text{Sr}$ ratio of the DCB extracts within Yedoma deposits. Such Yedoma formation should result in homogeneous radiogenic Sr isotopic signature with time. Note that slight differences might be explained by seasonal (summer and winter) variations in wind speed and directions likely modifying the origin of the loess material or by increased weathering before syngenetic freezing under warmer interstadial periods (Murton et al., 2015).

However, the identical $^{87}\text{Sr}/^{86}\text{Sr}$ ratio in DCB extracts between deposits that never thawed since deposition (Yedoma) and deposits that thawed during the Holocene (Alas and Lake sediment) was not expected. In this scenario where no change in Sr isotopic signature is found between Yedoma and previously thawed permafrost features, one cannot decipher no dissolution (scenario 1 in Fig. 1) or dissolution-precipitation of mineral OC interactions (scenario 2 in Fig. 1). Here, the identical Sr isotopic signature of the DCB extracts indicates that (i) mineral OC interactions were stable despite lake formation and drainage or (ii) mineral OC interactions were dissociated and subsequently precipitated with a Sr source with similar radiogenic Sr isotope ratio than at the time of the formation of the first mineral OC interaction. The fact that Alas deposits and Lake sediments are mainly composed of re-worked deposits from the former Yedoma deposits (Grosse et al., 2013) likely promoted an homogeneous $^{87}\text{Sr}/^{86}\text{Sr}$ ratio of the DCB extracts despite abrupt thaw processes.

4.2.2. Specific sediment layers

The maximum $^{87}\text{Sr}/^{86}\text{Sr}$ ratio of the DCB extracts from Duvanny Yar is found in a peat layer from the Yedoma profile (DY-01; 29 m a.r.l.) (Fig. 6a). The peat layer (10.5 wt% TOC) is a paleocryosol sequence with increased silt and lower sand content compared to other samples (mean grain size 16 μm ; Strauss (2010)). The increased TOC found in Yedoma deposits could be caused by ponding water and boggy conditions in low-center polygons under warmer conditions (Strauss et al., 2012). Such conditions could have promoted increased weathering and subsequent enrichment in resistant K-rich (more radiogenic) minerals. This specific layer is not characterized by an increase in Fe_d concentration but by an increase in Sr_d concentration (Fig. S7a). This could be evidence of increased mineral OC interactions in the form of organo-metallic complexes with Ca^{2+} and Sr^{2+} as previously hypothesized for Eight Mile Lake soils (section 4.1), and identified in deposits from the Yedoma domain (Monhonval et al., 2022). The contribution from Ca to OC complexes is likely not driven by pH conditions (not measured at the site but generally <7 in a peat layer). The accumulation of Ca available for OC complexation in a peat layer is likely related to plant cycling (Chapin et al., 1980), in line with the observations at the site of Eight Mile Lake (section 4.1.2).

In previously thawed deposits, the top layer from the Lake sediment profile displays the highest DCB-extracted $^{87}\text{Sr}/^{86}\text{Sr}$ ratio (Fig. 6d). This layer is dated from the Holocene period and results from peat formation processes. Like in the Yedoma profile DY-01, the highest radiogenic Sr isotopic ratio of the DCB extract is not concomitant with an increase in mineral OC interactions involving Fe (Fig. 6) but concomitant with a higher proportion of Sr participating in mineral OC interactions ($\text{Sr}_d/\text{Sr}_{\text{total}}$; Fig. S7d). This is supporting evidence for the importance of organo-metallic complexes with Ca^{2+} and Sr^{2+} .

4.3. Conditions for the preservation of mineral OC interactions upon permafrost thaw

4.3.1. Preservation of mineral OC interactions in saturated layers enriched in Fe-oxides and organo-metallic complexes

In soils from Eight Mile Lake, specific layers from the saturated active layer are Fe_d enriched and display a different radiogenic Sr signature of the DCB extract than layers above or below (Fig. 4e, f, c for soil profiles with increasing active layer depth Ext1 < Ext3 < Mod2). These Fe_d

enriched layers are located below the water table level at the time of sampling (Table S2). Given the long-term fluctuations of the water table with permafrost thaw at the site (Schoor et al., 2021), these layers may reflect past redox interfaces corresponding to past water table. However, these layers today are not affected by repetitive redox fluctuations. A shorter soil water residence time limits shifts in redox conditions, and there is a contrast in water saturation conditions between poorly (minimal lateral drainage) and deeply (drainage more rapid) thawed profiles (Hirst et al., 2022). Despite these contrasts in water saturation along the thaw gradient, the data suggest a preservation of the Sr isotopic signature from the time of the formation of the mineral OC interactions in these Fe_d enriched layers, and hence a stability of mineral OC interactions upon permafrost thaw. In parallel, specific peat layers from Yedoma domain deposits (layers with the highest TOC values in Fig. S2a, b, d) with no Fe_d accumulation (Fig. 6a, b, d) suggest mineral OC interactions such as organo-metallic complexes involving Ca^{2+} and Sr^{2+} rather than the Fe cations. The highest Sr isotopic ratios of the DCB extracts observed in these peat layers (Fig. 6a, b, d) are concomitant with an increase in Sr_d (Fig. S7 a, b, d), likely involved as organo-metallic complexes rather than occluded or adsorbed to Fe oxides. The observations from the two sites (Eight Mile Lake and Duvanny Yar) imply that Fe_d enriched saturated layers or peat layers may offer stable conditions for mineral OC interactions and could mitigate the OC vulnerability to permafrost thaw (Fig. 7), as supported by previous studies (Monhonval et al., 2021b; Joss et al., 2022).

The Fe_d enriched saturated layer in the deeply thawed profile Mod2 (10–15 cm; Fig. 4c) is well suited to quantify the stability of mineral OC interactions in waterlogged conditions. This specific layer is not classified as organic-rich (TOC = 8 wt%, i.e., below the cutoff at 20% for organic rich layers) but shows concomitant increase in Fe_d and $^{87}Sr/^{86}Sr$ ratio of the DCB extract. This layer displays a Sr isotopic ratio of 0.7094107. According to Eq. (1), this indicates that 21% of the Sr originates from the permafrost layer and 79% from the top surface layer. In comparison, the unsaturated active layer in Mod2 on average is

characterized by 85% of the Sr with a permafrost isotopic signature and only 15% from the top unsaturated active layer. The increase in mineral OC interaction and subsequent increase in the $^{87}Sr/^{86}Sr$ ratio of the DCB extract raised the amount of the stable pool of Sr that remained undissociated in mineral OC interaction compared to other layers with a lower potential for mineral OC interactions. These calculations indicate that 79% of Sr trapped in mineral OC interactions originates from the top surface layer when there is an accumulation of mineral OC interactions, but this proportion decreases to 15% in layers without mineral OC interactions accumulation. By difference between these two pools, this suggests that 64% of the Sr originating from top layer was preserved thanks to the accumulation of mineral OC interactions. The same calculation can be applied to the accumulation peak of mineral OC interactions in profile Ext1 and Ext3: this supports that 51% of the Sr originates from the upper part of the profile at Fe_d accumulation peak against 47% on average in the saturated layer for Ext1, and 38% against 20% on average in the saturated layer for Ext3. By difference between the area of Fe_d accumulation and the average of the saturated zone, overall this indicates that in that layer between 4% and 64% of mineral OC interactions have remained undissociated since their formation.

4.3.2. Dissolution-precipitation of mineral OC interactions at redox interfaces

Despite the significant accumulation of Fe_d indicating increasing mineral OC interactions at the redox interface of Eight Mile Lake soils, no change in $^{87}Sr/^{86}Sr$ ratio of the DCB extracts in these layers relative to their surrounding layers is observed (Fig. 7). The redox interface acts as an oxidative barrier that promotes Fe oxides precipitation with potential co-precipitation of Sr. The Fe_d accumulation found at the redox interface is the result of redox shift due to water table fluctuations and reported in many studies (Lipson et al., 2012; Riedel et al., 2013; Herndon et al., 2017; Patzner et al., 2022). Our approach is consistent with the observations from Wortberg et al. (2017) using radiogenic Sr isotopes to trace the source of Fe aggregates co-precipitated with Sr in rivers and

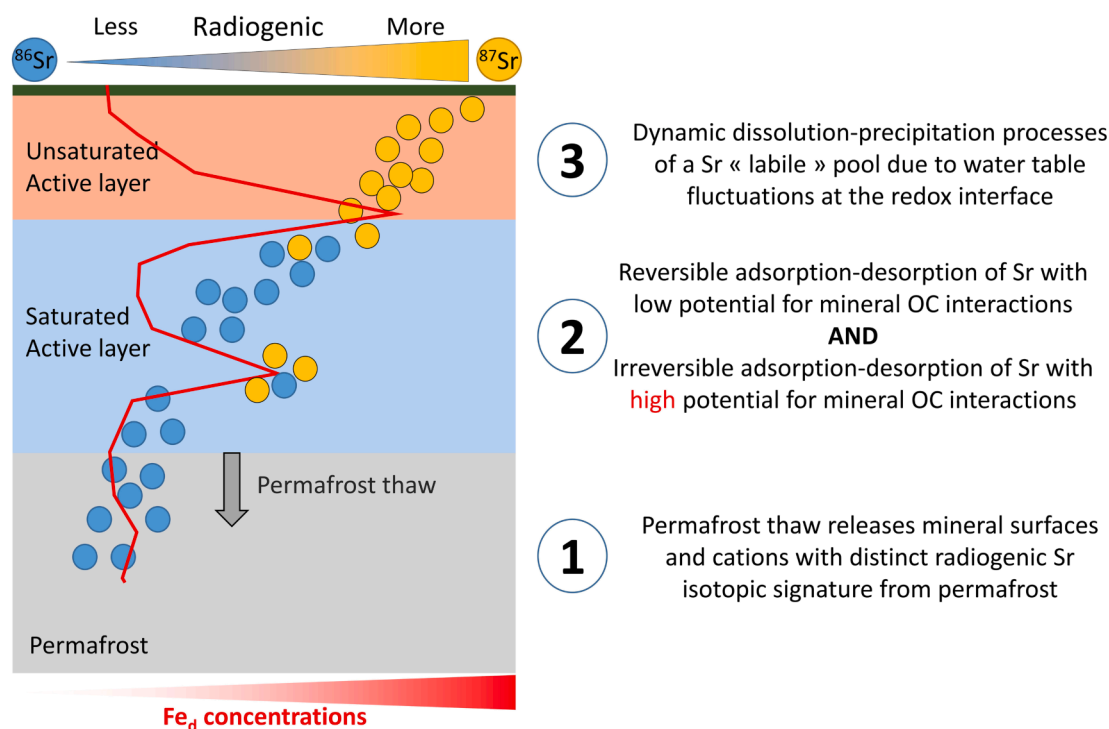


Fig. 7. Schematic of permafrost soil radiogenic Sr isotope ratio in the DCB extract (blue and yellow Sr isotopes) and concentration in DCB-extracted Fe (Fe_d ; red line) dynamic upon thaw. At the boundary between saturated and unsaturated soil layers (i.e., redox interface), the accumulation of Fe_d is not correlated with a change in radiogenic Sr ratio in the DCB extract. In saturated soil layer, the increase in Fe_d is concomitant with an increase in radiogenic Sr ratio in the DCB extract indicating a stable pool of Sr with a conservative property in mineral OC interactions rich layers.

originating from a redox interface between anoxic groundwater and oxic stream water. Here, to explain the unchanged Sr isotopic ratio at redox interface in soil layers characterized with little Fe oxides and mainly organo-metallic complexes accumulation, we argue that the ongoing aerobic-anaerobic conditions promoted by water table fluctuations induces persistent and dynamic dissolution-precipitation of mineral OC interactions. In turn, this would favor an increased proportion of a labile Sr pool vulnerable to dissolution and a precipitation of new mineral OC interactions, contrasting with the stable Sr pool from saturated layers (section 4.3.1).

In parallel, the accumulation of Fe_d in previously thawed profiles from the Yedoma domain (Fig. 6) can also be explained by Fe redistribution and precipitation where local conditions favors oxidation reactions (Monhonval et al., 2021b). The increase in Fe_d concentration without change in radiogenic Sr isotopic ratio is similar than what is observed at the redox interface of Eight Mile Lake. Therefore, this could be explained by similar processes of ongoing dissolution-precipitation processes in layers with mineral OC interactions accumulation promoting the formation of a Sr highly “labile” pool. Note that this could also be explained by the homogeneous Sr isotopic ratio with depth in both Yedoma and previously thawed profiles.

Overall, the lack of difference in ⁸⁷Sr/⁸⁶Sr ratio of the DCB extracts between layers accumulating Fe-oxides at redox interfaces regularly affected by water table changes (or upon thermokarst processes) relative to surrounding layers supports the dominance of a Sr “labile” pool inherited from processes of dissolution and precipitation of the mineral OC interactions characterized with a signature from the local environment (Fig. 7).

4.3.3. Increasing contribution from mineral weathering to mineral OC interactions upon gradual permafrost thaw

In Eight Mile Lake soils, profiles can be divided as poorly thawed (Min1, Mod1 and Ext1; <60 cm active layer thickness) or deeply thawed (Mod2, Mod3, Ext3; >60 cm). Using a mixing equation identical to Eq. (1) (section 4.3.1), we can determine the proportion of Sr adsorbed or occluded to Fe oxides and participating in organo-metallic complexes which found its source from the less radiogenic minerals in permafrost layers compared to the more radiogenic unsaturated layers. On average, the saturated active layer of poorly thawed soil profiles is characterized by a higher radiogenic Sr ratio of the DCB extracts (0.7091367 ± 0.000485 , $n = 10$) than the saturated active layer from deeply thawed profiles (0.7087963 ± 0.000661 , $n = 15$; p -value < 0.05; Fig. S6a). According to calculation based on Eq.1, 53% of Sr in mineral OC interactions in the saturated layer of poorly thawed profiles is from permafrost layers in Min1 and Ext1 (Mod1 is left out because no samples are located in the saturated layer) while in deeply thawed profiles, this contribution increases to >80% (85% in Mod2, 100% in Mod3, 80% in Ext3). This higher contribution of less radiogenic Sr in mineral OC interactions in deeply thawed soil profiles is direct evidence of the contribution of mineral elements from newly thawed layers (weatherable minerals) to OC stabilization mechanisms. This hypothesis is supported by the two-fold higher values of Total Reserve in Bases (TRB = total concentration in Ca + Mg + K + Na; Herbillon, 1986) in saturated active layer from deeply thawed profile (Mod3 and Ext3 with TRB of 186 and 184 cmol_c kg⁻¹, respectively; Mauclet et al., 2023) compared to the saturated soil layer from poorly thawed profile (Min1 = 77 cmol_c kg⁻¹; Mauclet et al., 2023). The higher TRB value from deeply thawed profiles directly supports a larger weatherable mineral reserve in these soils originating from newly thawed poorly weathered soil layer, i.e., a direct source of Sr included in mineral OC interactions.

A mixing model using radiogenic Sr ratio is a powerful tool to estimate the contribution of different Sr source when end-members are clearly defined with different Sr isotopic signature and when additional end-members are not left out of the mixing model. We acknowledge that the end-members defined in this study have significantly different radiogenic Sr ratio (p -value < 0.001; Eq. (1)) but display a high

variability within permafrost (0.7087378 ± 0.000625 ; mean \pm 2SD). End-members are critical in mixing models and further investigations to define narrower ranges for the radiogenic Sr isotope composition of the Sr sources participating in mineral OC interactions in different permafrost systems might help to better constrain dissolution-precipitation processes of these mineral OC interactions as proposed in this study.

5. Conclusions

In conclusion, we found that:

(i) In saturated soil layers of tundra soils vulnerable to gradual thaw, the accumulation of mineral OC interactions is correlated with a more radiogenic Sr isotope signature in DCB extracts targeting mineral OC interactions. This supports that between 4% and 64% of mineral OC interactions have remained undissociated since their formation, and preserve a “stable” pool of Sr.

(ii) At the redox interface of tundra soils accumulating mineral OC interactions, the absence of change in the radiogenic Sr ratio of DCB extracts supports that the redox shift induced by fluctuating water table level promotes dynamic dissolution-precipitation of mineral OC interactions. This likely promotes a large contribution of a Sr “labile” pool reflecting the radiogenic Sr signature of the surrounding layers.

(iii) Ongoing permafrost thaw releases minerals likely to get involved in organic carbon stabilization mechanisms. This is supported by a larger contribution of Sr with a permafrost signature in mineral OC interactions in deeply thawed soils (>80%) than in poorly thawed soils (~53%).

(iv) In Yedoma deposits vulnerable to abrupt thaw such as thermokarst lake formation and drainage, the similar range of Sr isotopic signature of the DCB extracts in the deposits prior and after thawing did not allow us to determine whether or not the mineral OC interactions have been modified upon thermokarst process. Either mineral OC interactions are stable upon thermokarst process or, after Fe oxide dissolution or organo-metallic complexes dissociation, the newly available Sr occluded upon Fe oxide precipitation or complexed with OC display a similar radiogenic Sr ratio than the previous Sr source.

In perspective, this first attempt to use radiogenic Sr isotopes in dithionite-citrate-bicarbonate extracts to trace the *in-situ* dissolution-precipitation processes of mineral OC interactions is promising and should be tested in other thawing permafrost features. Future research directions should investigate potential limitations related to the sensitivity of the approach to (i) Fe associated mineral OC interactions relative to Ca associated complexes and to (ii) redox-sensitive newly precipitated Fe associated OC.

Declaration of Competing Interest

The authors declare that they have no known competing financial interests or personal relationships that could have appeared to influence the work reported in this paper.

Data availability

All data are provided in the [Supplementary material](#)

Acknowledgements

We thank Elisabeth Mauclet, Simon Malvaux and Justin Ledman for their help on the field and Emily Stevenson for her help with the Sr isotope methodology, H el ene Dailly and the Mineral and Organic Chemical Analysis (MOCA) platform from UCLouvain for the chemical and isotopic analysis, Aubry Vandeuren and Beno ıt Pereira for their expertise on portable X-ray Fluorescence, and S ebastien Fran ois and the technical unit from Earth and Life Institute environment (ELIE) for their help with the steel pipe sampling device construction. We acknowledge the associate editor Alberto Agnelli and two anonymous

reviewers for their constructive comments. We thank Guido Grosse and Lutz Schirmer for their expertise on the site of Duvanny Yar, a work embedded into the Action Group “The Yedoma Region” funded by the International Permafrost Association, and ECOSS in Flagstaff for their expertise on Eight Mile Lake study site. This work was supported by the European Union’s Horizon 2020 research and innovation program [grant agreement No. 714617] to SO, and SO acknowledges funding from the Fund for Scientific Research FNRS in Belgium [FC69480].

Appendix A. Supplementary data

Supplementary data to this article can be found online at <https://doi.org/10.1016/j.geoderma.2023.116456>.

References

- Aciego, S.M., Bourdon, B., Lupker, M., Rickli, J., 2009. A new procedure for separating and measuring radiogenic isotopes (U, Th, Pa, Ra, Sr, Nd, Hf) in ice cores. *Chem. Geol.* 266 (3–4), 194–204.
- Alekseev, A., Alekseeva, T., Ostroumov, V., Siegert, C., Gradusov, B., 2003. Mineral transformations in permafrost-affected soils, North Kolyma Lowland, Russia. *Soil Sci. Soc. Am. J.* 67, 596. <https://doi.org/10.2136/sssaj2003.0596>.
- Andersson, P.S., Wasserburg, G.J., Ingri, J., Stordal, M.C., 1994. Strontium, dissolved and particulate loads in fresh and brackish waters: the Baltic Sea and Mississippi Delta. *Earth Planet. Sci. Lett.* 124, 195–210. [https://doi.org/10.1016/0012-821X\(94\)00062-X](https://doi.org/10.1016/0012-821X(94)00062-X).
- Bagard, M.-L., Schmitt, A.-D., Chabaux, F., Pokrovsky, O.S., Viers, J., Stille, P., Labolle, F., Prokushkin, A.S., 2013. Biogeochemistry of stable Ca and radiogenic Sr isotopes in a larch-covered permafrost-dominated watershed of Central Siberia. *Geochim. Cosmochim. Acta* 114, 169–187. <https://doi.org/10.1016/j.gca.2013.03.038>.
- Banner, J.L., 2004. Radiogenic isotopes: systematics and applications to earth surface processes and chemical stratigraphy. *Earth Sci. Rev.* 65, 141–194. [https://doi.org/10.1016/S0012-8252\(03\)00086-2](https://doi.org/10.1016/S0012-8252(03)00086-2).
- Bascomb, C.L., 1968. Distribution of pyrophosphate-extractable iron and organic carbon in soils of various groups. *J. Soil Sci.* 19, 251–268. <https://doi.org/10.1111/j.1365-2389.1968.tb01538.x>.
- Biskaborn, B.K., Herzschuh, U., Bolshiyakov, D.Y., Schwamborn, G., Diekmann, B., 2013. Thermokarst processes and depositional events in a Tundra Lake, Northeastern Siberia: Thermokarst processes in a Siberian tundra lake. *Permafrost. Periglacial Process.* 24, 160–174. <https://doi.org/10.1002/ppp.1769>.
- Capo, R.C., Stewart, B.W., Chadwick, O.A., 1998. Strontium isotopes as tracers of ecosystem processes: theory and methods. *Geoderma* 82, 197–225. [https://doi.org/10.1016/S0016-7061\(97\)00102-X](https://doi.org/10.1016/S0016-7061(97)00102-X).
- Chadwick, O.A., Derry, L.A., Bern, C.R., Vitousek, P.M., 2009. Changing sources of strontium to soils and ecosystems across the Hawaiian Islands. *Chem. Geol.* 267 (1–2), 64–76.
- Chapin, F.S., Johnson, D.A., McKendrick, J.D., 1980. Seasonal movement of nutrients in plants of differing growth form in an Alaskan tundra ecosystem: implications for herbivory. *J. Ecol.* 68, 189–209.
- Colombo, C., Palumbo, G., He, J.-Z., Pinton, R., Cesco, S., 2014. Review on iron availability in soil: interaction of Fe minerals, plants, and microbes. *J. Soils Sediments* 14, 538–548. <https://doi.org/10.1007/s11368-013-0814-z>.
- Derry, L.A., Chadwick, O.A., 2007. Contributions from Earth’s atmosphere to soil. *Elements* 3 (5), 333–338.
- Drouet, T., Herbauts, J., Gruber, W., Demaiffe, D., 2007. Natural strontium isotope composition as a tracer of weathering patterns and of exchangeable calcium sources in acid leached soils developed on loess of central Belgium. *Eur. J. Soil Sci.* 58, 302–319. <https://doi.org/10.1111/j.1365-2389.2006.00840.x>.
- Faure, G., Powell, J.L., 1972. *Strontium Isotope Geology, Minerals, Rocks and Mountains*. Springer-Verlag, Berlin Heidelberg. <https://doi.org/10.1007/978-3-642-65367-4>.
- Fox-Kemper, B., Hewitt, H.T., Xiao, C., Aðalgeirsdóttir, G., Drijfhout, S.S., Edwards, T.L., Gollgedge, N.R., Hemer, M., Kopp, R.E., Krinner, G., Mix, A., Notz, D., Nowicki, S., Nurhati, I.S., Ruiz, L., Sallée, J.-B., Slangen, A.B.A., Yu, Y., 2021. Ocean, Cryosphere and Sea Level Change, in: Masson-Delmotte, V., Zhai, P., Pirani, A., Connors, S.L., Péan, C., Berger, S., Caud, N., Chen, Y., Goldfarb, L., Gomis, M.L., Huang, M., Leitzell, K., Lonnoy, E., Matthews, J.B.R., Maycock, T.K., Waterfield, T., Yelekci, O., Yu, R., Zhou, B. (Eds.), *Climate Change 2021: The Physical Science Basis*. Contribution of Working Group I to the Sixth Assessment Report of the Intergovernmental Panel on Climate Change. Cambridge University Press, Cambridge, United Kingdom and New York, NY, USA, pp. 1211–1362. <https://doi.org/10.1017/9781009157896.011>.
- Gentsch, N., Wild, B., Mikutta, R., Čapek, P., Diáková, K., Schrumpp, M., Turner, S., Minnich, C., Schaarschmidt, F., Šhibistova, O., Schnecker, J., Ulrich, T., Gittel, A., Šantrůčková, H., Bárta, J., Lashchinskiy, N., Fuß, R., Richter, A., Guggenberger, G., 2018. Temperature response of permafrost soil carbon is attenuated by mineral protection. *Glob. Chang. Biol.* 24, 3401–3415. <https://doi.org/10.1111/gcb.14316>.
- Graustein, W.C., Armstrong, R.L., 1983. The use of strontium-87/strontium-86 ratios to measure atmospheric transport into forested watersheds. *Science* 219 (4582), 289–292.
- Grosse, G., Jones, B., Arp, C., 2013. *Thermokarst Lakes, Drainage, and Drained Basins, in: Treatise on Geomorphology*. Elsevier, pp. 325–353. <https://doi.org/10.1016/B978-0-12-374739-6.00216-5>.
- Gupta, D.K., Deb, U., Walther, C., Chatterjee, S., 2018. Strontium in the Ecosystem: Transfer in Plants via Root System. In: Gupta, D.K., Walther, C. (Eds.), *Behaviour of Strontium in Plants and the Environment*. Springer International Publishing, Cham, pp. 1–18. https://doi.org/10.1007/978-3-319-66574-0_1.
- Hemingway, J.D., Rothman, D.H., Grant, K.E., Rosengard, S.Z., Eglinton, T.I., Derry, L.A., Galy, V.V., 2019. Mineral protection regulates long-term global preservation of natural organic carbon. *Nature* 570, 228–231. <https://doi.org/10.1038/s41586-019-1280-6>.
- Herbillon, A.J., 1986. Chemical estimation of weatherable minerals present in the diagnostic horizons of low activity clay soils, in: *Proceedings of the 8th International Clay Classification Workshop: Classification, Characterization and Utilization of Oxisols (Part 1)*[Beinroth, FH, Camargo, MN and Eswaran (Ed.)][39–48](Rio de Janeiro, 1986).
- Herndon, E., Albashaireh, A., Singer, D., Roy Chowdhury, T., Gu, B., Graham, D., 2017. Influence of iron redox cycling on organo-mineral associations in Arctic tundra soil. *Geochim. Cosmochim. Acta* 207, 210–231. <https://doi.org/10.1016/j.gca.2017.02.034>.
- Hicks Pries, C.E., Schuur, E.A.G., Crummer, K.G., 2012. Holocene carbon stocks and carbon accumulation rates altered in soils undergoing permafrost thaw. *Ecosystems* 15, 162–173. <https://doi.org/10.1007/s10021-011-9500-4>.
- Hirst, C., Mauclet, E., Monhonval, A., Tihon, E., Ledman, J., Schuur, E.A.G., Opfergelt, S., 2022. Seasonal changes in hydrology and permafrost degradation control mineral element-bound DOC transport from permafrost soils to streams. *Global Biogeochem. Cycles* 36. <https://doi.org/10.1029/2021GB007105>.
- Hutchings, J.A., Bianchi, T.S., Kaufman, D.S., Kholodov, A.L., Vaughn, D.R., Schuur, E.A.G., 2019. Millennial-scale carbon accumulation and molecular transformation in a permafrost core from Interior Alaska. *Geochim. Cosmochim. Acta* 253, 231–248. <https://doi.org/10.1016/j.gca.2019.03.028>.
- IUSS Working Group WRB, 2015. *World Reference Base for Soil Resources 2014, update 2015 International soil classification system for naming soils and creating legends for soil maps*. World Soil Resources Reports.
- Joss, H., Patzner, M.S., Maisch, M., Mueller, C.W., Kappler, A., Bryce, C., 2022. Cryoturbation impacts iron-organic carbon associations along a permafrost soil chronosequence in northern Alaska. *Geoderma* 413, 115738. <https://doi.org/10.1016/j.geoderma.2022.115738>.
- Keil, R.G., Mayer, L.M., 2014. *Mineral Matrices and Organic Matter, in: Treatise on Geochemistry*. Elsevier, pp. 337–359. <https://doi.org/10.1016/B978-0-08-095975-7.01024-X>.
- Keller, K., Blum, J.D., Kling, G.W., 2007. Geochemistry of Soils and Streams on Surfaces of Varying Ages in Arctic Alaska. *Arct. Antarct. Alp. Res.* 39, 84–98. [https://doi.org/10.1657/1523-0430\(2007\)39\[84:GOSASO\]2.0.CO;2](https://doi.org/10.1657/1523-0430(2007)39[84:GOSASO]2.0.CO;2).
- Keller, K., Blum, J.D., Kling, G.W., 2010. Stream geochemistry as an indicator of increasing permafrost thaw depth in an arctic watershed. *Chem. Geol.* 273, 76–81. <https://doi.org/10.1016/j.chemgeo.2010.02.013>.
- Kleber, M., Bourg, I.C., Coward, E.K., Hansel, C.M., Myneni, S.C.B., Nunan, N., 2021. Dynamic interactions at the mineral–organic matter interface. *Nat. Rev. Earth Environ.* 2 (6), 402–421.
- Kleber, M., Eusterhues, K., Keiluweit, M., Mikutta, C., Mikutta, R., Nico, P.S., 2015. Mineral–Organic Associations: Formation, Properties, and Relevance in Soil Environments, in: *Advances in Agronomy*. Elsevier, pp. 1–140. <https://doi.org/10.1016/bs.agron.2014.10.005>.
- Kokelj, S.V., Lacelle, D., Lantz, T.C., Tunnicliffe, J., Malone, L., Clark, I.D., Chin, K.S., 2013. Thawing of massive ground ice in mega slumps drives increases in stream sediment and solute flux across a range of watershed scales: FLUVIAL IMPACTS OF THERMOKARST. *J. Geophys. Res. Earth* 118, 681–692. <https://doi.org/10.1002/jgrf.20063>.
- Lipson, D.A., Zona, D., Raab, T.K., Bozzolo, F., Mauritz, M., Oechel, W.C., 2012. Water-table height and microtopography control biogeochemical cycling in an Arctic coastal tundra ecosystem. *Biogeosciences* 9, 577–591. <https://doi.org/10.5194/bg-9-577-2012>.
- Mauclet, E., Agnan, Y., Hirst, C., Monhonval, A., Pereira, B., Vandeuren, A., Villani, M., Ledman, J., Taylor, M., Jasinski, B.L., Schuur, E.A.G., Opfergelt, S., 2022. Changing sub-Arctic tundra vegetation upon permafrost degradation: impact on foliar mineral element cycling. *Biogeosciences* 19, 2333–2351. <https://doi.org/10.5194/bg-19-2333-2022>.
- Mauclet, E., Hirst, C., Monhonval, A., Stevenson, E.I., Gérard, M., Villani, M., Dailly, H., Schuur, E.A.G., Opfergelt, S., 2023. Tracing changes in base cation sources for Arctic tundra vegetation upon permafrost thaw. *Geoderma* 429, 116277. <https://doi.org/10.1016/j.geoderma.2022.116277>.
- Mehra, O.P., Jackson, M.L., 1960. Iron oxide removal from soils and clays by a dithionite-citrate system buffered with sodium bicarbonate. *Proc. 7th Natl. Conf. Clays Clay Minerals* 317–327. <https://doi.org/10.1016/B978-0-08-009235-5.50026-7>.
- Miller, E.K., Blum, J.D., Friedland, A.J., 1993. Determination of soil exchangeable-cation loss and weathering rates using Sr isotopes. *Nature* 362, 438–441. <https://doi.org/10.1038/362438a0>.
- Monhonval, A., Mauclet, E., Pereira, B., Vandeuren, A., Strauss, J., Grosse, G., Schirmer, L., Fuchs, M., Kuhry, P., Opfergelt, S., 2021a. Mineral element stocks in the yedoma domain: a novel method applied to ice-rich permafrost regions. *Front. Earth Sci.* 9, 773. <https://doi.org/10.3389/feart.2021.703304>.
- Monhonval, A., Strauss, J., Mauclet, E., Hirst, C., Bemelmans, N., Grosse, G., Schirmer, L., Fuchs, M., Opfergelt, S., 2021b. Iron redistribution upon

- Thermokarst processes in the Yedoma domain. *Front. Earth Sci.* <https://doi.org/10.3389/feart.2021.703339>.
- Monhonval, A., Strauss, J., Thomas, M., Hirst, C., Titeux, H., Louis, J., Gilliot, A., du Bois d'Aische, E., Pereira, B., Vandeuken, A., Grosse, G., Schirmermeister, L., Jongejans, L.L., Ulrich, M., Opfergelt, S., 2022. Thermokarst processes increase the supply of stabilizing surfaces and elements (Fe, Mn, Al, and Ca) for mineral-organic carbon interactions. *Permafrost. Periglac. Process.* 33 (4), 452–469.
- Mu, C.C., Zhang, T.J., Zhao, Q., Guo, H., Zhong, W., Su, H., Wu, Q.B., 2016. Soil organic carbon stabilization by iron in permafrost regions of the Qinghai-Tibet Plateau. *Geophys. Res. Lett.* 43, 10286–10294. <https://doi.org/10.1002/2016GL070071>.
- Murton, J.B., Goslar, T., Edwards, M.E., Bateman, M.D., Danilov, P.P., Savvinov, G.N., Gubin, S.V., Ghaleb, B., Haile, J., Kanevskiy, M., Lozhkin, A.V., Lupachev, A.V., Murton, D.K., Shur, Y., Tikhonov, A., Vasil'chuk, A.C., Vasil'chuk, Y.K., Wolfe, S.A., 2015. Palaeoenvironmental Interpretation of Yedoma Silt (Ice Complex) Deposition as Cold-Climate Loess, Duvanny Yar, Northeast Siberia. *Permafrost. Periglac. Process.* 26 (3), 208–288.
- Opfergelt, S., 2020. The next generation of climate model should account for the evolution of mineral-organic interactions with permafrost thaw. *Environ. Res. Lett.* 15 (9), 091003. <https://doi.org/10.1088/1748-9326/ab9a6d>.
- Osterkamp, T.E., Jorgenson, M.T., Schuur, E.A.G., Shur, Y.L., Kanevskiy, M.Z., Vogel, J. G., Tumskey, V.E., 2009. Physical and ecological changes associated with warming permafrost and thermokarst in Interior Alaska. *Permafrost Periglac. Process.* 20, 235–256. <https://doi.org/10.1002/ppp.656>.
- Palmtag, J., Ramage, J., Hugelius, G., Gentsch, N., Lashchinskiy, N., Richter, A., Kuhry, P., 2016. Controls on the storage of organic carbon in permafrost soil in northern Siberia: soil organic carbon storage in permafrost terrain, northern Siberia. *Eur. J. Soil Sci.* 67, 478–491. <https://doi.org/10.1111/ejss.12357>.
- Parfitt, R.L., Childs, C.W., 1988. Estimation of forms of Fe and Al - a review, and analysis of contrasting soils by dissolution and Mossbauer methods. *Soil Res.* 26, 121–144. <https://doi.org/10.1071/sr9880121>.
- Patzner, M.S., Mueller, C.W., Malusova, M., Baur, M., Nikeleit, V., Scholten, T., Hoeschen, C., Byrne, J.M., Borch, T., Kappler, A., Bryce, C., 2020. Iron mineral dissolution releases iron and associated organic carbon during permafrost thaw. *Nat. Commun.* 11, 6329. <https://doi.org/10.1038/s41467-020-20102-6>.
- Patzner, M.S., Kainz, N., Lundin, E., Barczok, M., Smith, C., Herndon, E., Kinsman-Costello, L., Fischer, S., Straub, D., Kleindienst, S., Kappler, A., Bryce, C., 2022. Seasonal fluctuations in iron cycling in thawing permafrost peatlands. *Environ. Sci. Technol.* 56, 4620–4631. <https://doi.org/10.1021/acs.est.1c06937>.
- Pearce, C.R., Parkinson, J.J., Gaillardet, J., Charlier, B.L., Mokadem, F., Burton, K.W., 2015. Reassessing the stable (888/86Sr) and radiogenic (87Sr/86Sr) strontium isotopic composition of marine inputs. *Geochim. Cosmochim. Acta* 157, 125–146.
- Plaza, C., Pegoraro, E., Bracho, R., Celis, G., Crummer, K.G., Hutchings, J.A., Hicks Pries, C.E., Mauritz, M., Natali, S.M., Salmon, V.G., Schädel, C., Webb, E.E., Schuur, E.A.G., 2019. Direct observation of permafrost degradation and rapid soil carbon loss in tundra. *Nat. Geosci.* 12 (8), 627–631. <https://doi.org/10.1038/s41561-019-0387-6>.
- Popov, A.I., 1953. Lithogenesis of alluvial lowlands in the cold climatic conditions. *Izvestiya (Transactions) of the USSR Academy of Sciences. Geography* 2, 29–41.
- R Core Team, 2018. *R: A Language and Environment for Statistical Computing*. R Foundation for Statistical Computing, Vienna, Austria.
- Rennert, T., 2019. Wet-chemical extractions to characterise pedogenic Al and Fe species – a critical review. *Soil Res.* 57, 1. <https://doi.org/10.1071/SR18299>.
- Reyes, F.R., Loughheed, V.L., 2015. Rapid nutrient release from permafrost thaw in arctic aquatic ecosystems. *Arct. Antarct. Alp. Res.* 47, 35–48. <https://doi.org/10.1657/AAAR0013-099>.
- Riedel, T., Zak, D., Biester, H., Dittmar, T., 2013. Iron traps terrestrially derived dissolved organic matter at redox interfaces. *Proc. Natl. Acad. Sci. USA* 110 (25), 10101–10105.
- Rodenhizer, H., Ledman, J., Mauritz, M., Natali, S.M., Pegoraro, E., Plaza, C., Romano, E., Schädel, C., Taylor, M., Schuur, E., 2020. Carbon thaw rate doubles when accounting for subsidence in a permafrost warming experiment. *J. Geophys. Res. Biogeosci.* 125 <https://doi.org/10.1029/2019JG005528>.
- Rowley, M.C., Grand, S., Verrecchia, E.P., 2018. Calcium-mediated stabilisation of soil organic carbon. *Biogeochemistry* 137, 27–49. <https://doi.org/10.1007/s10533-017-0410-1>.
- Rozenbaum, G.E., Shpolyanskaya, N.A., 1998. Late Cenozoic permafrost history of the Russian Arctic. *Permafrost. Periglac. Process.* 9 (3), 247–273.
- Schuur, E.A.G., Crummer, K.G., Vogel, J.G., Mack, M.C., 2007. Plant Species Composition and Productivity following Permafrost Thaw and Thermokarst in Alaskan Tundra. *Ecosystems* 10, 280–292. <https://doi.org/10.1007/s10021-007-9024-0>.
- Schuur, E.A.G., McGuire, A.D., Schädel, C., Grosse, G., Harden, J.W., Hayes, D.J., Hugelius, G., Koven, C.D., Kuhry, P., Lawrence, D.M., Natali, S.M., Olefeldt, D., Romanovsky, V.E., Schaefer, K., Turetsky, M.R., Treat, C.C., Vonk, J.E., 2015. Climate change and the permafrost carbon feedback. *Nature* 520, 171–179. <https://doi.org/10.1038/nature14338>.
- Schuur, E.A.G., Bracho, R., Celis, G., Belshe, E.F., Ebert, C., Ledman, J., Mauritz, M., Pegoraro, E.F., Plaza, C., Rodenhizer, H., Romanovsky, V., Schädel, C., Schirokauer, D., Taylor, M., Vogel, J.G., Webb, E.E., 2021. Tundra underlain by thawing permafrost persistently emits carbon to the atmosphere over 15 years of measurements. *J. Geophys. Res. Biogeosci.* 126 <https://doi.org/10.1029/2020JG006044>.
- Schwertmann, U., 1991. Solubility and dissolution of iron oxides. *Plant Soil* 130, 1–25. <https://doi.org/10.1007/BF00011851>.
- Shmelev, D., Cherbunina, M., Rogov, V., Opfergelt, S., Monhonval, A., Strauss, J., 2021. Reconstructing permafrost sedimentological characteristics and post-depositional processes of the Yedoma Stratotype Duvanny Yar, Siberia. *Front. Earth Sci.* 9. <https://doi.org/10.1002/feart.2021.703339>.
- Smalley, I.J., Smalley, V., 1983. Loess Material and Loess Deposits: Formation, Distribution and Consequences, in: Brookfield, M.E., Ahlbrandt, T.S. (Eds.), *Developments in Sedimentology, Eolian Sediments and Processes*. Elsevier, pp. 51–68. [https://doi.org/10.1016/S0070-4571\(08\)70788-X](https://doi.org/10.1016/S0070-4571(08)70788-X).
- Strauss, J., 2010. *Late Quaternary Environmental Dynamics at the Duvanny Yar key Section, Lower Kolyma*. Universität Potsdam, Potsdam, East Siberia.
- Strauss, J., Schirmermeister, L., Wetterich, S., Borchers, A., Davydov, S.P., 2012. Grain-size properties and organic-carbon stock of Yedoma Ice Complex permafrost from the Kolyma lowland, northeastern Siberia. *Global Biogeochem. Cycles* 26. <https://doi.org/10.1029/2011GB004104>.
- Strauss, J., Schirmermeister, L., Grosse, G., Fortier, D., Hugelius, G., Knoblauch, C., Romanovsky, V., Schädel, C., Schneider von Deimling, T., Schuur, E.A.G., Shmelev, D., Ulrich, M., Veremeeva, A., 2017. Deep Yedoma permafrost: a synthesis of depositional characteristics and carbon vulnerability. *Earth Sci. Rev.* 172, 75–86. <https://doi.org/10.1016/j.earscirev.2017.07.007>.
- Strauss, J., Abbott, B., Hugelius, G., Schuur, E.A.G., Treat, C., Fuchs, M., Schädel, C., Ulrich, M., Turetsky, M., Keuschnig, M., Biasi, C., Yang, Y., Grosse, G., 2021. Permafrost, in: *Recarbonizing global soils – A technical manual of recommended management practices*. In: edited by: Food and Agriculture Organization of the United Nations (FAO), pp. 127–147. <https://doi.org/10.4060/cb6378en>.
- Street, L.E., Dean, J.F., Billett, M.F., Baxter, R., Dinsmore, K.J., Lessels, J.S., Subke, J.-A., Tetzlaff, D., Wookey, P.A., 2016. Redox dynamics in the active layer of an Arctic headwater catchment; examining the potential for transfer of dissolved methane from soils to stream water. *J. Geophys. Res. Biogeosci.* 121, 2776–2792. <https://doi.org/10.1002/2016JG003387>.
- Stumm, W., Sulzberger, B., 1992. The cycling of iron in natural environments: considerations based on laboratory studies of heterogeneous redox processes. *Geochim. Cosmochim. Acta* 56, 3233–3257. [https://doi.org/10.1016/0016-7037\(92\)90301-X](https://doi.org/10.1016/0016-7037(92)90301-X).
- Tomirdjaro, S.V., Chernen'kiy, O., 1987. Cryogenic deposits of East Arctic and Sub Arctic. -AN SSSR Far-East-Science Centre 196 pp.
- van Huissteden, J., 2020. In: *Thawing Permafrost: Permafrost Carbon in a Warming Arctic*. Springer International Publishing, Cham. <https://doi.org/10.1007/978-3-030-31379-1>.
- Villani, M., Maucllet, E., Agnan, Y., Druel, A., Jasinski, B., Taylor, M., Schuur, E.A.G., Opfergelt, S., 2022. Mineral element recycling in topsoil following permafrost degradation and a vegetation shift in sub-Arctic tundra. *Geoderma* 421, 115915. <https://doi.org/10.1016/j.geoderma.2022.115915>.
- von Lützow, M., Kogel-Knabner, I., Ekschmitt, K., Matzner, E., Guggenberger, G., Marschner, B., Flessa, H., 2006. Stabilization of organic matter in temperate soils: mechanisms and their relevance under different soil conditions - a review. *Eur. J. Soil Sci.* 57, 426–445. <https://doi.org/10.1111/j.1365-2389.2006.00809.x>.
- Vonk, J.E., Tank, S.E., Walvoord, M.A., 2019. Integrating hydrology and biogeochemistry across frozen landscapes. *Nat. Commun.* 10, 5377. <https://doi.org/10.1038/s41467-019-13361-5>.
- Winkler, P., Kaiser, K., Thompson, A., Kalbitz, K., Fiedler, S., Jahn, R., 2018. Contrasting evolution of iron phase composition in soils exposed to redox fluctuations. *Geochim. Cosmochim. Acta* 235, 89–102. <https://doi.org/10.1016/j.gca.2018.05.019>.
- Wortberg, K., Conrad, S., Andersson, P.S., Ingri, J., 2017. Strontium isotopes – A tracer for river suspended iron aggregates. *Appl. Geochem.* 79, 85–90. <https://doi.org/10.1016/j.apgeochem.2017.02.012>.
- Zanina, O.G., Gubin, S.V., Kuzmina, S.A., Maximovich, S.V., Lopatina, D.A., 2011. Late-Pleistocene (MIS 3–2) palaeoenvironments as recorded by sediments, palaeosols, and ground-squirrel nests at Duvanny Yar, Kolyma lowland, northeast Siberia. *Quat. Sci. Rev.* 30, 2107–2123. <https://doi.org/10.1016/j.quascirev.2011.01.021>.